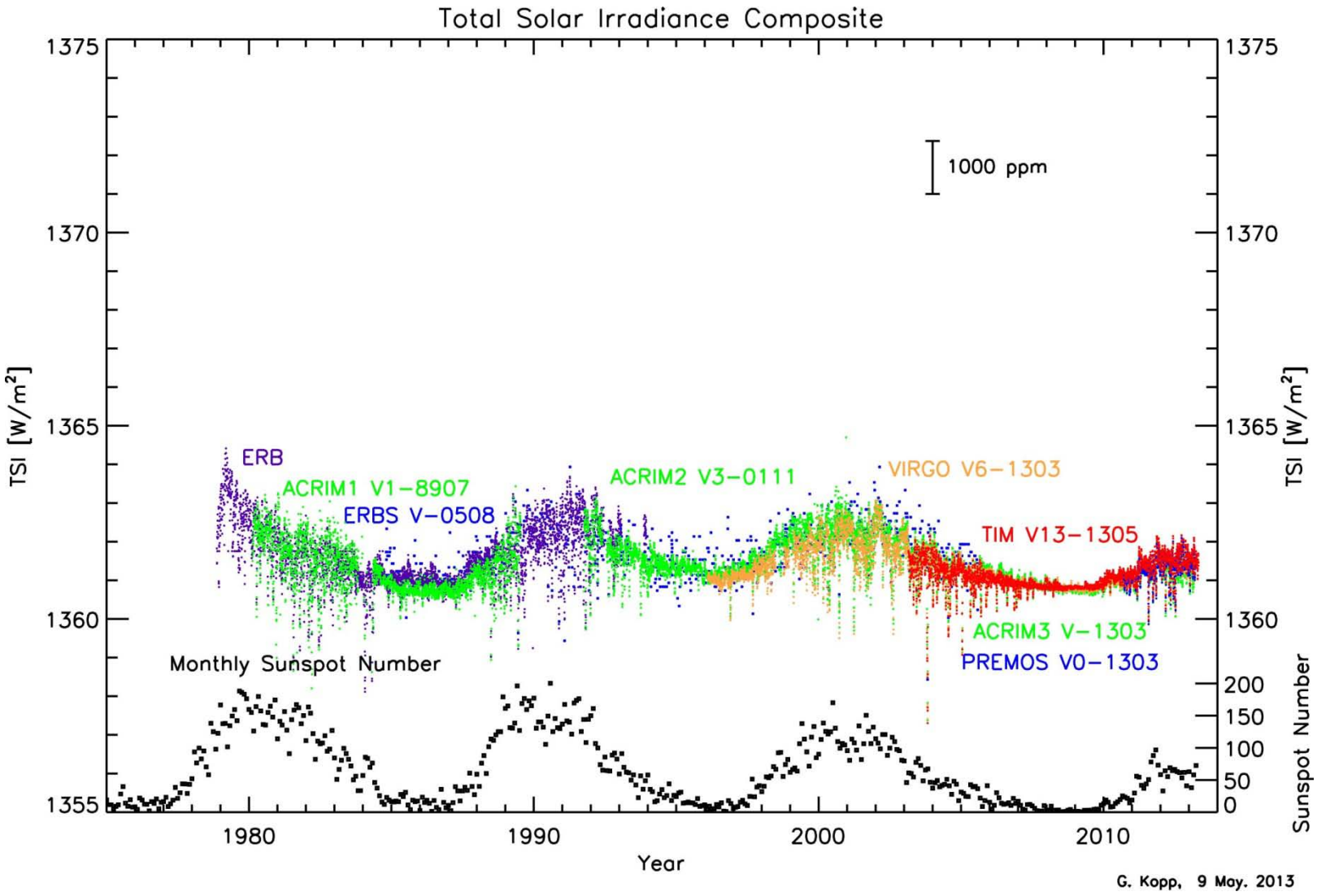

Figure 5.1 Composite record of Total Solar Irradiance, TSI (the 'Solar Constant') from 1975 to 2013 compiled from multiple satellite radiometric measurements adjusted to a standard reference scale. Also shown is the monthly mean sunspot number, illustrating the strong correlation with TSI (Data courtesy of Greg Kopp, NASA, http://spot.colorado.edu/~koppg/TSI/)

Table 5.1 Distribution of Energy in the Spectrum Emitted by the Sun

Waveband (nm)	**Energy (%)**
0–200	0.7
200–280 (UV-C)	0.5
280–320 (UV-B)	1.5
320–400 (UV-A)	6.3
400–700 (visible/PAR)	39.8
700–1500 (near-infra-red)	38.8
$1500 - \infty$	12.4

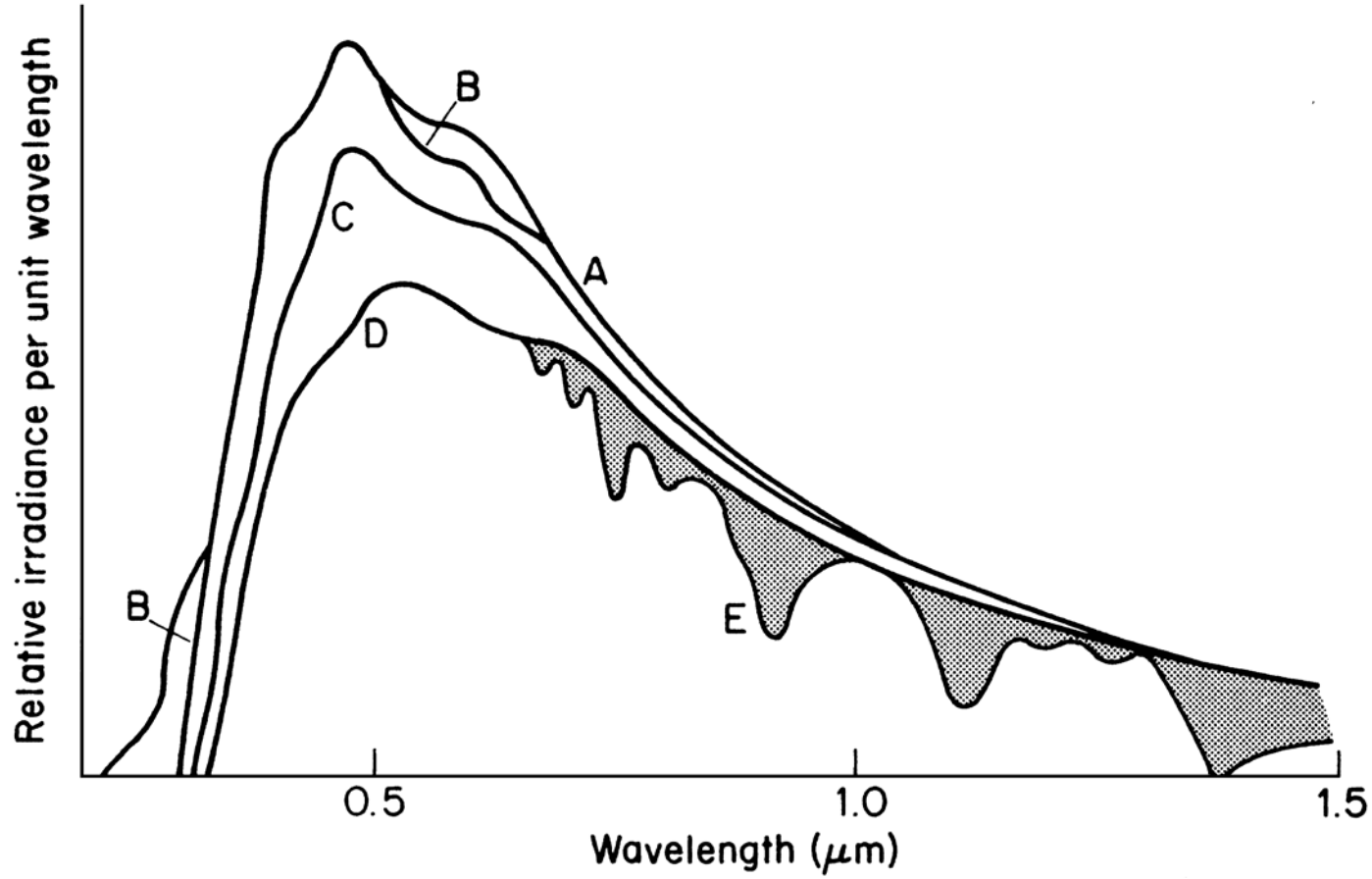

Figure 5.2 Successive processes attenuating the solar beam as it penetrates the atmosphere. A---extraterrestrial radiation, B---after ozone absorption, C---after molecular scattering, D---after aerosol scattering, E---after water vapor and oxygen absorption (from Henderson, 1977).

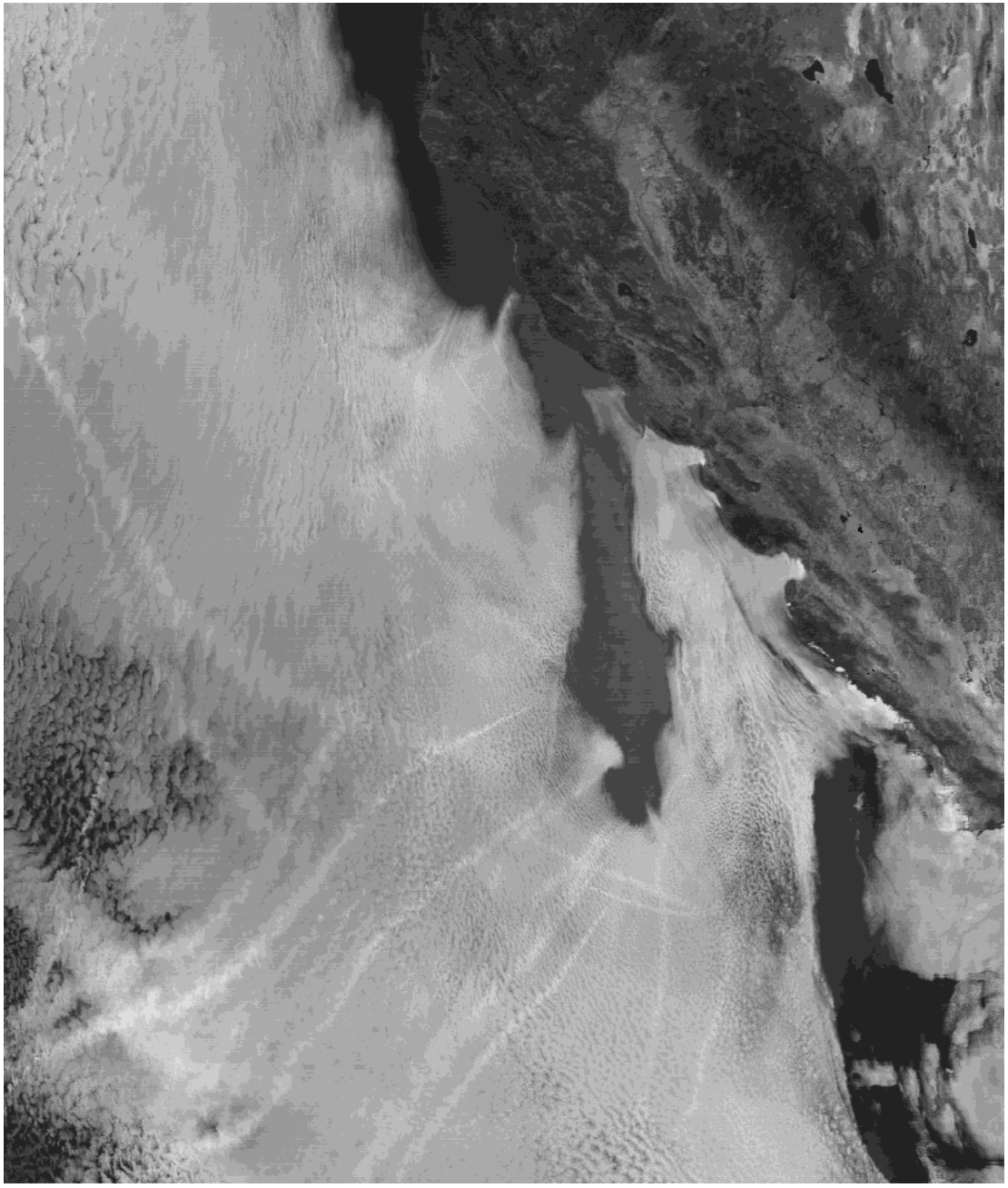

Figure 5.3 Infrared satellite image of reflected solar radiation at 2.1µm off the coast of California near San Francisco. Pollution from ship smoke emissions increases the reflectivity of marine stratus clouds by supporting the formation of larger numbers of smaller droplets than in unpolluted cloud nearby. This enables ship tracks to be seen clearly in the image. Courtesy of Dr. J Coakley.

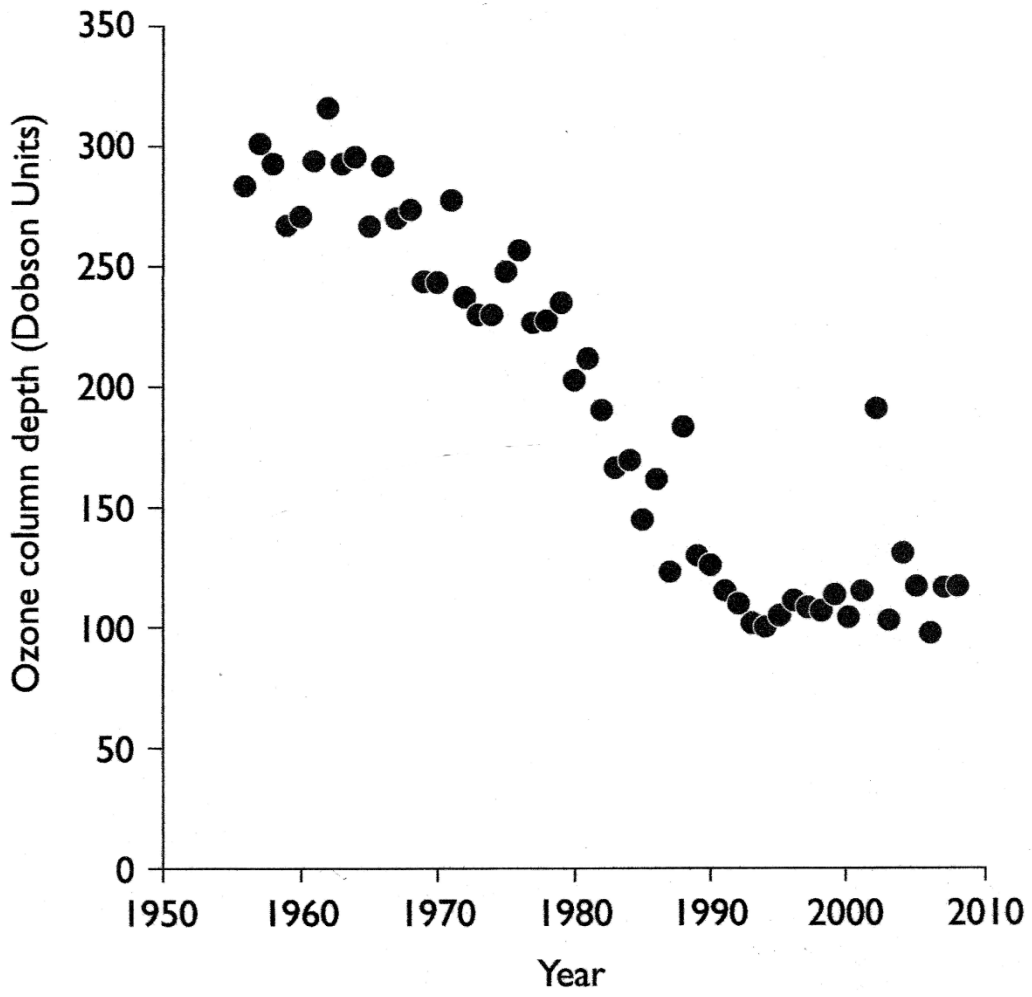

Figure 5.4 Minimum October ozone column depth at the British Antarctic Survey research station, Halley Bay, Antarctica from 1956 to 2009. (1 Dobson Unit corresponds to a layer of gaseous ozone 10μm thick at STP). (data courtesy of the British Antarctic Survey)

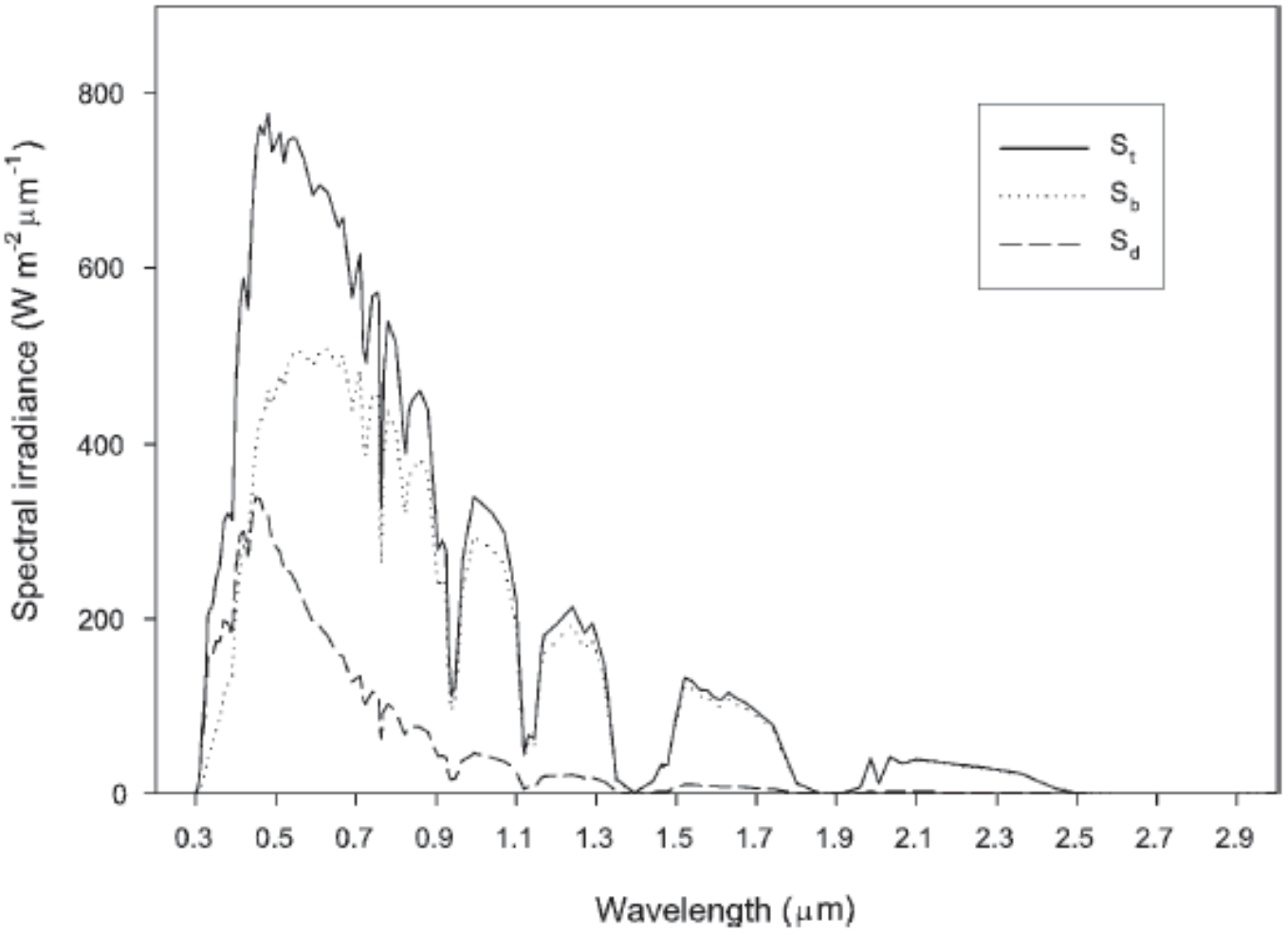

Figure 5.5 Spectral distribution of direct, $\mathbf{S}_b$, diffuse, $\mathbf{S}_d$, and total solar radiation, $\mathbf{S}_t$ on a horizontal surface, calculated using a simple model of a cloudless atmosphere (courtesy of the Solar Energy Research Institute; see Bird and Riordan 1984). Solar zenith angle is 60° (m=2), precipitable water is 20 mm, ozone thickness is 3mm, and aerosol optical depth is 0.2. Note that the diffuse flux has maximum energy per unit wavelength at about 0.46 μm.

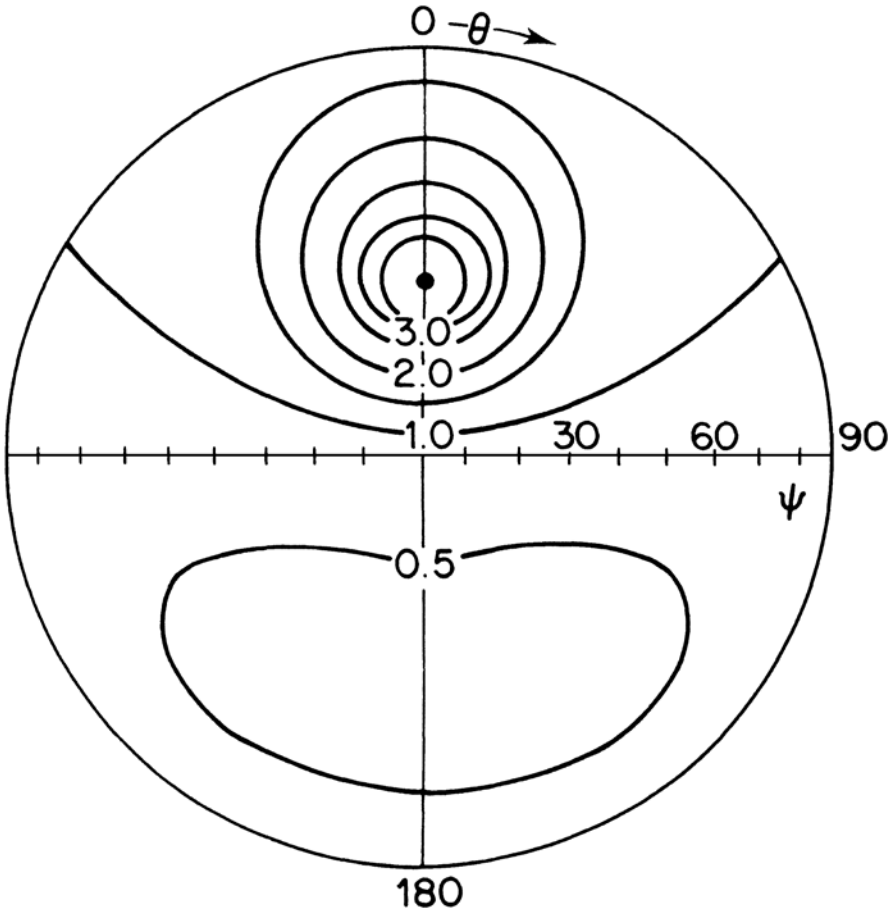

Figure 5.6 Standard distribution of normalized sky radiance $\pi N/S_d$ for solar zenith angle 35°, where N is the value of sky radiance at a point and πN is the diffuse flux which the surface would receive if the whole sky were uniformly bright (see p. 46) (from Steven, 1977).

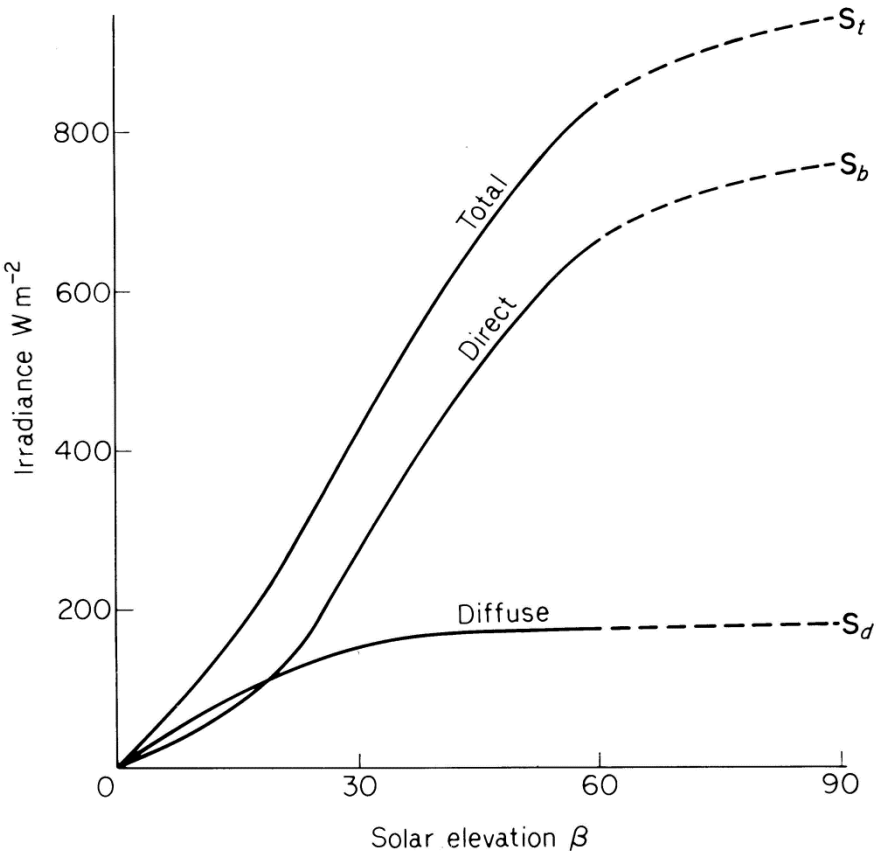

Figure 5.7 Solar irradiance on a cloudless day (16 July 1969) at Sutton Bonington (53° N, 1° W): $\mathbf{S}_t$ total flux; $\mathbf{S}_d$ diffuse flux, $\mathbf{S}_b$ direct flux on a horizontal surface.

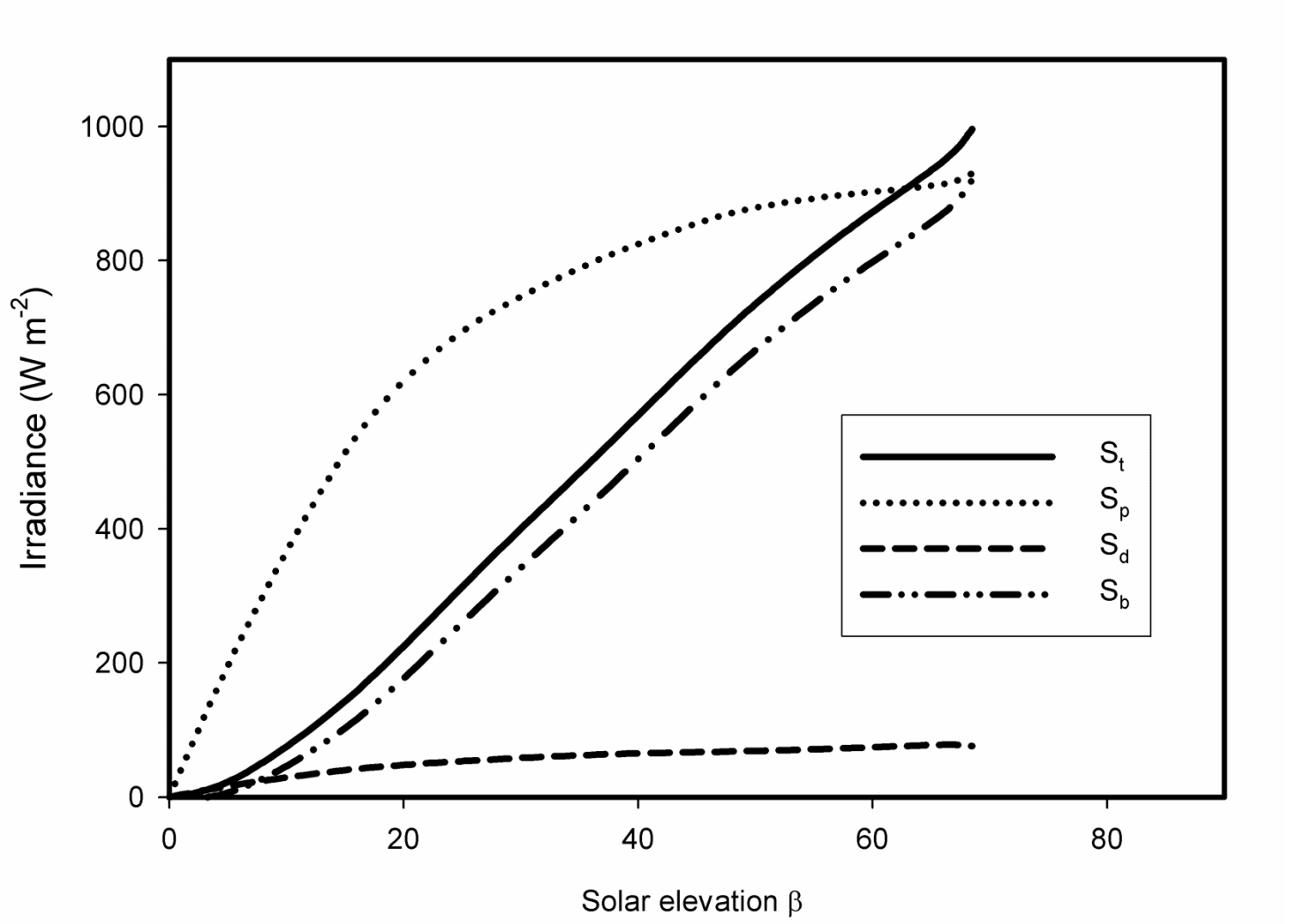

Figure 5.8 Solar irradiance on a cloudless day (12 June 2002) at Eugene,Oregon (44◦N, 123◦W): $\mathbf{S}_t$ total flux; $\mathbf{S}_d$ diffuse flux; $\mathbf{S}_b$ direct flux on a horizontal surface. The curve labeled $\mathbf{S}_p$ is the direct flux at normal incidence. (Data courtesy of Frank Vignola, University of Oregon.)

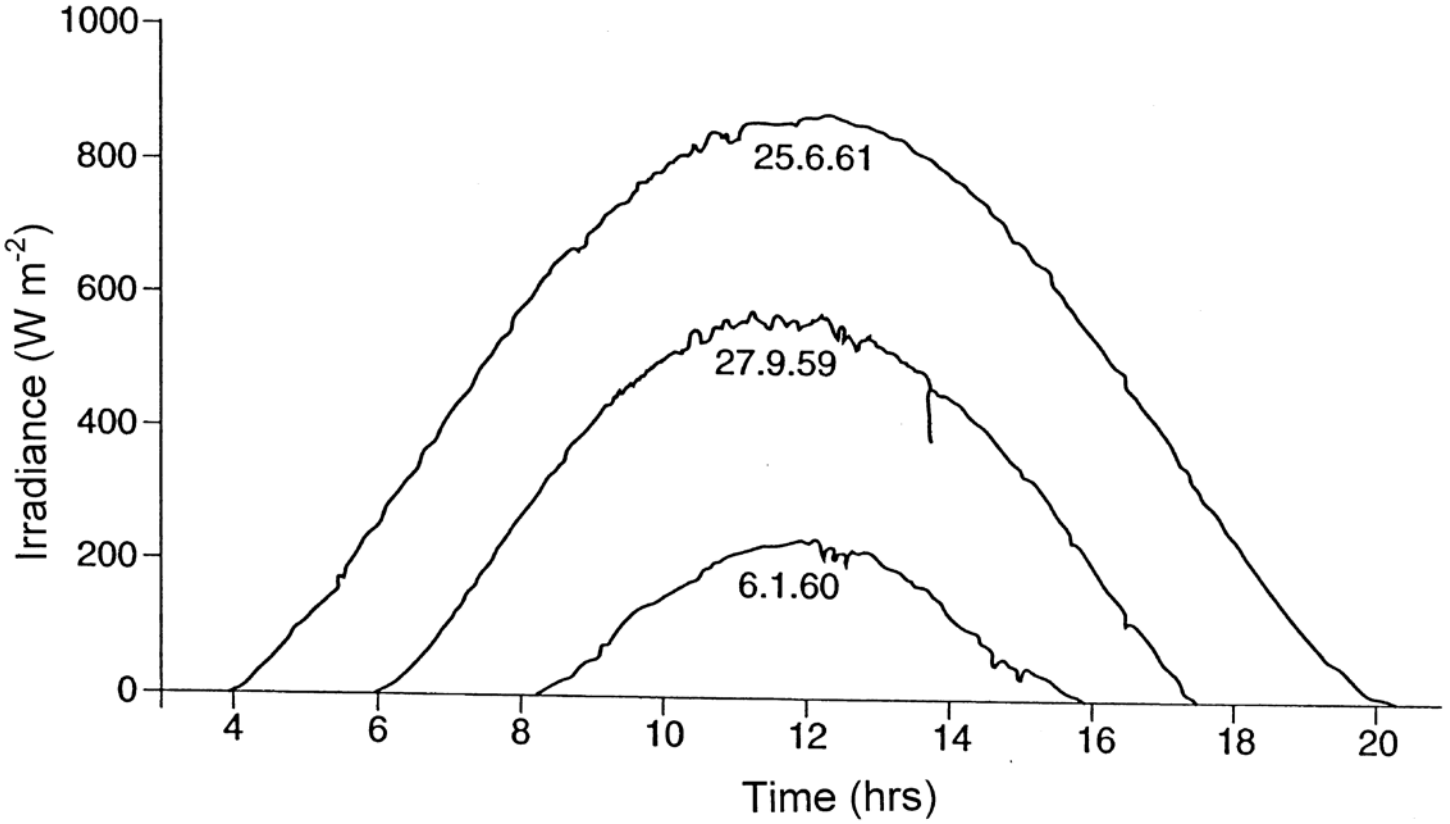

Figure 5.9 Solar radiation on three cloudless days at Rothamsted, England (52°N, 0°W).During The middle of the day, the record tends to fluctuate more than in the morning and evening, suggesting a diurnal change in the amount of dust in the lower atmosphere, at least in summer and autumn.

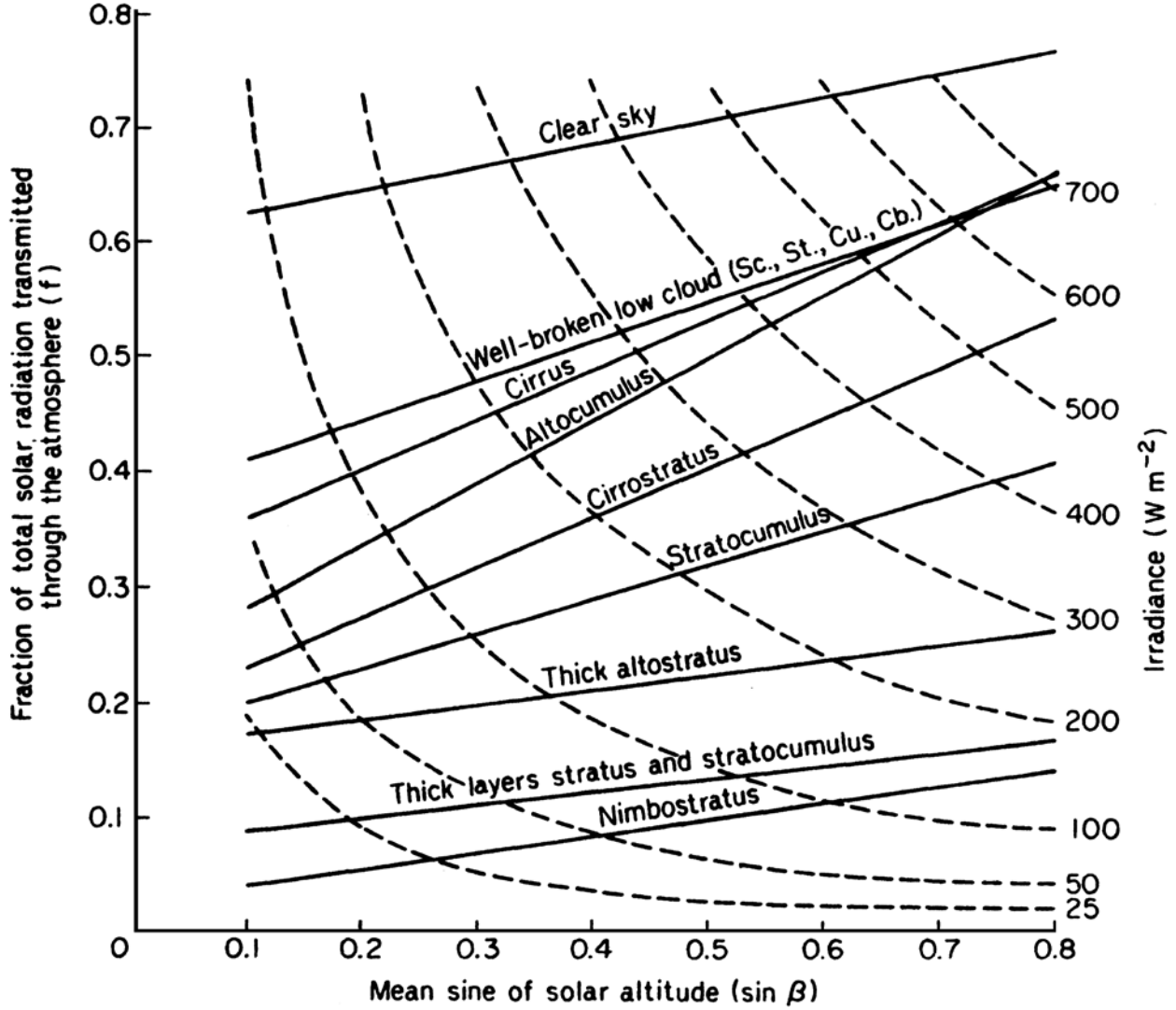

Figure 5.10 Empirical relations between solar radiation and solar angle for different cloud types from measurements in the North Atlantic (52°N, 20°W). The curves are isopleths of irradiance (from Lumb, 1964). Sc, stratocumulus; St, stratus; Cu, cumulus; Cb, cumulonimbus.

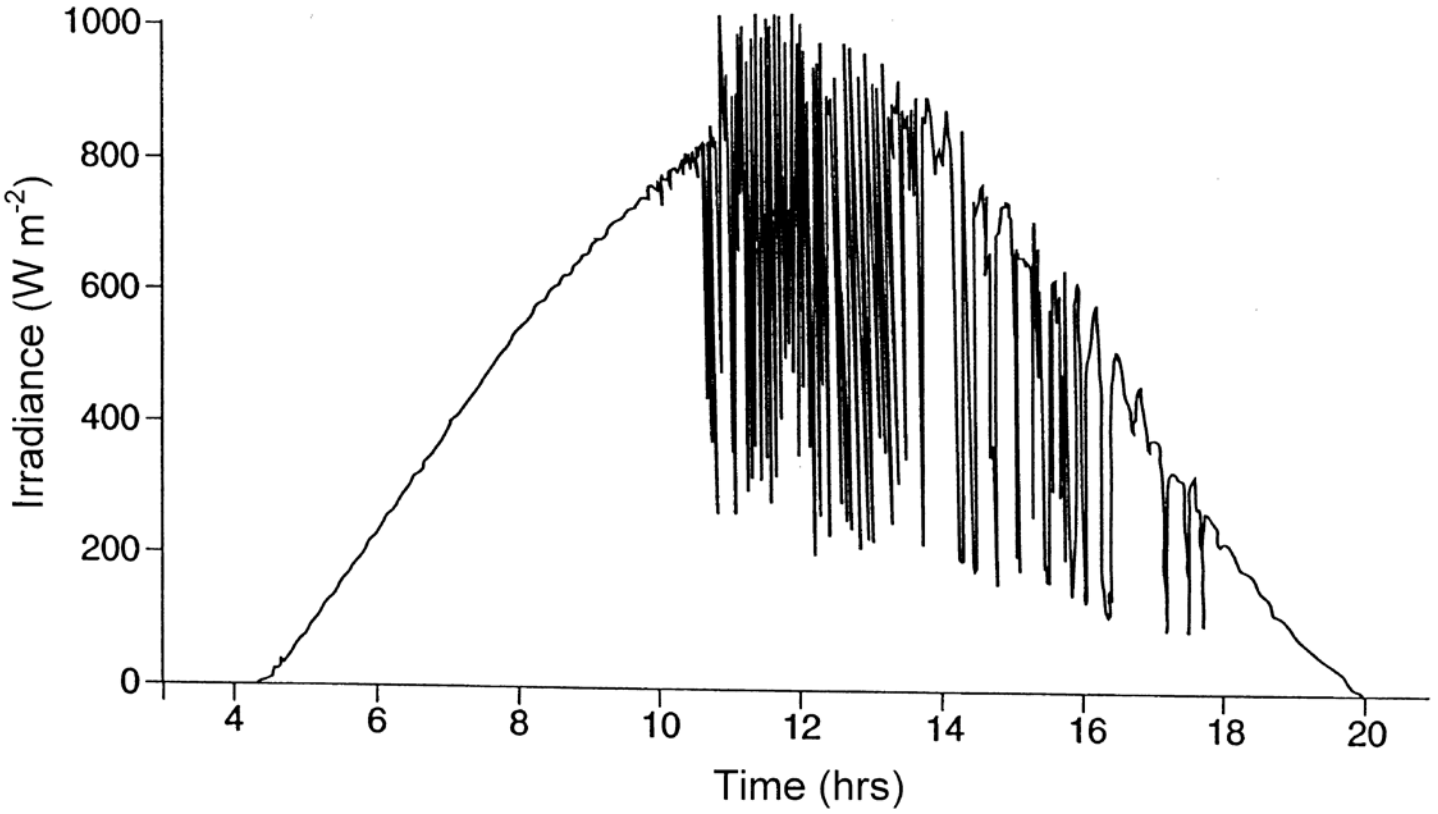

Figure 5.11 Solar radiation on a day of broken cloud (11 June 1969) at Rothamsted, England (52°N, 0°W). Note very high values of irradiance immediately before and after occlusion of the sun by cloud and the regular succession of minimum values when the sun is completely obscured.

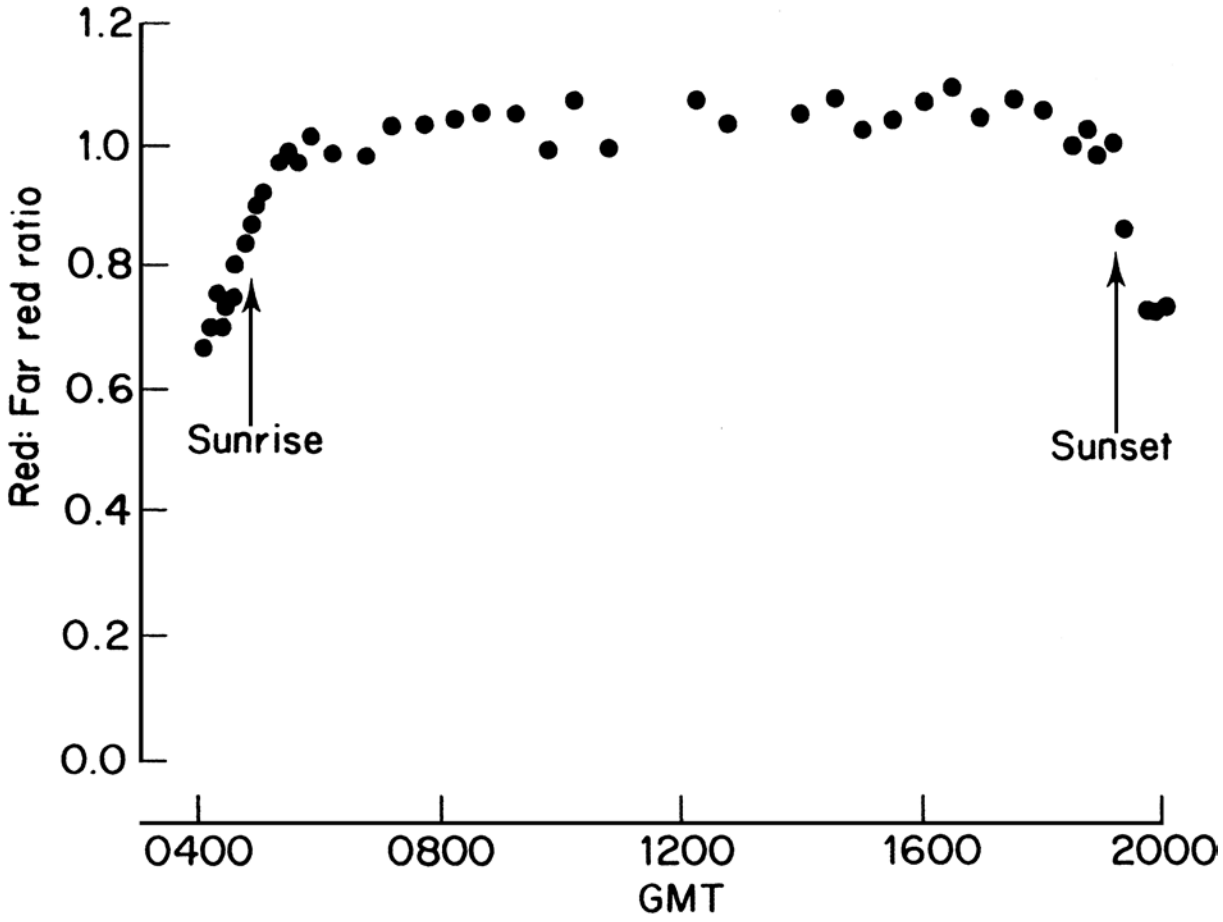

Figure 5.12 Ratio of spectral irradiance at 660 nm (red) to spectral irradiance at 730 nm (far-red) on an overcast day (25 August 1980) near Leicester in the English Midlands (from Smith and Morgan, 1981).

Table 5.2 Short-Wave Radiation Balance of Atmosphere and Surface at Kew Observatory (51.5°N) for 1956–1960 Expressed as a Percentage of Extraterrestrial Flux

	Winter (Nov–Jan)	Spring (Feb–Apr)	Summer (May–Jul)	Autumn (Aug–Oct)	Year
Extraterrestrial radiation (ET)					
Seasonal total (MJ m^{-2})	800	2050	3720	2340	8910
Daily mean (MJ m^{-2} day^{-1})	8.7	22.3	40.4	25.4	24.4
Losses in the atmosphere (%ET)					
(a) Absorption					
Water vapor	15	12	13	15	13
Cloud	8	9	9	9	9
Dust and smoke	15	10	5	8	8
Total	38%	31%	27%	32%	30%
(b) Scattering (away from surface)	37%	35%	33%	34%	34%
Radiation at surface (%ET)					
Direct	8	14	18	14	15
Diffuse	17	20	22	20	21
Total	25%	34%	40%	34%	36%
	100%	100%	100%	100%	100%
Total as MJ m^{-2} day^{-1}	2.2	7.6	16.2	8.7	8.8

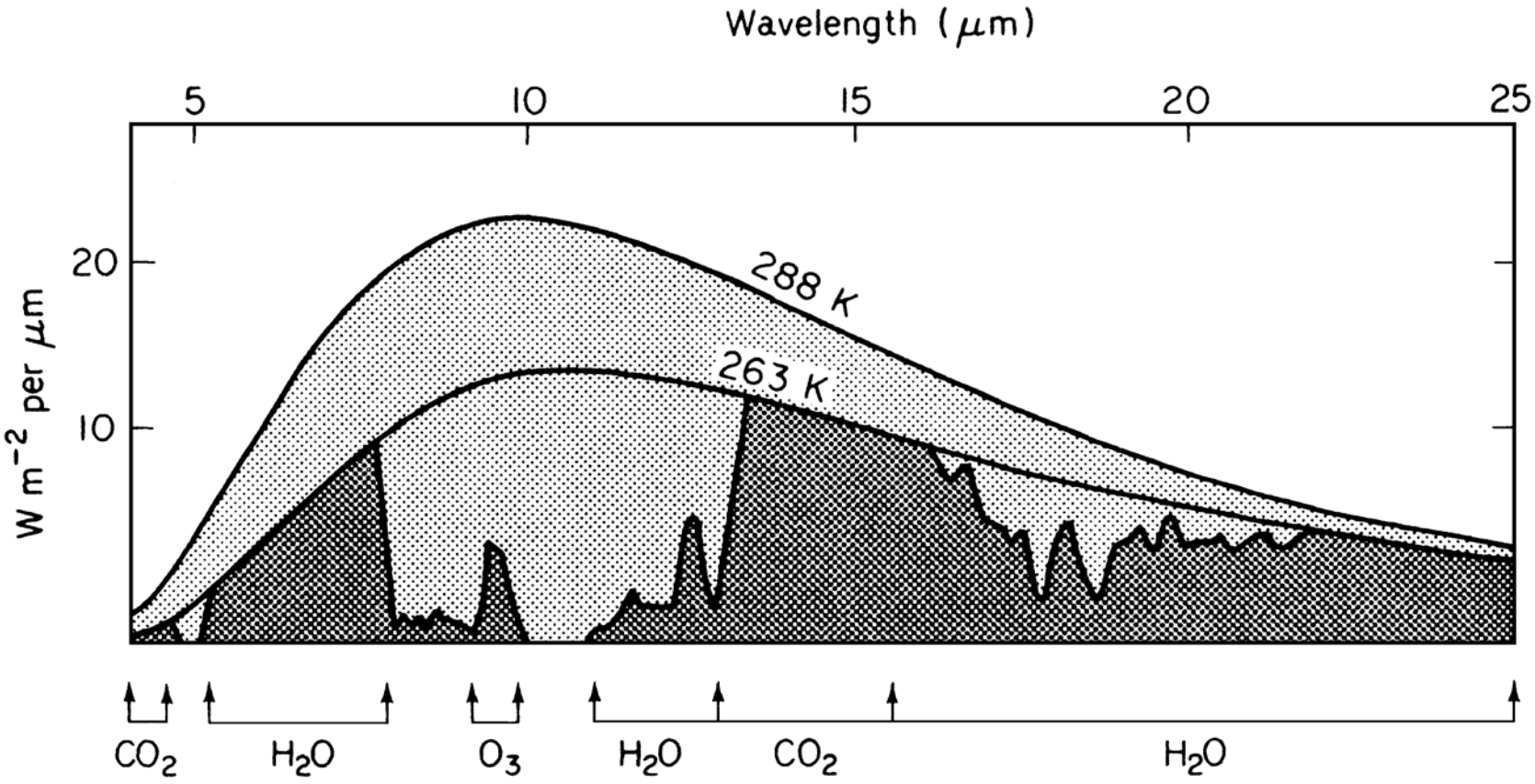

Figure 5.13 Spectral distribution of long-wave radiation for black bodies at 298 K and 263 K. Dark gray areas show the emission from atmospheric gases at 263 K. The light gray area therefore shows the net loss of radiation from a surface at 288 K to a cloudless atmosphere at a uniform temperature of 263 K (after Gates, 1980).

Figure 5.14 Black-body radiation at T_a (full circles) and long-wave radiation from clear sky (open circles) from Eq. (5.25). Straight lines are approximations from Equations (5.26) and (5.27) respectively.

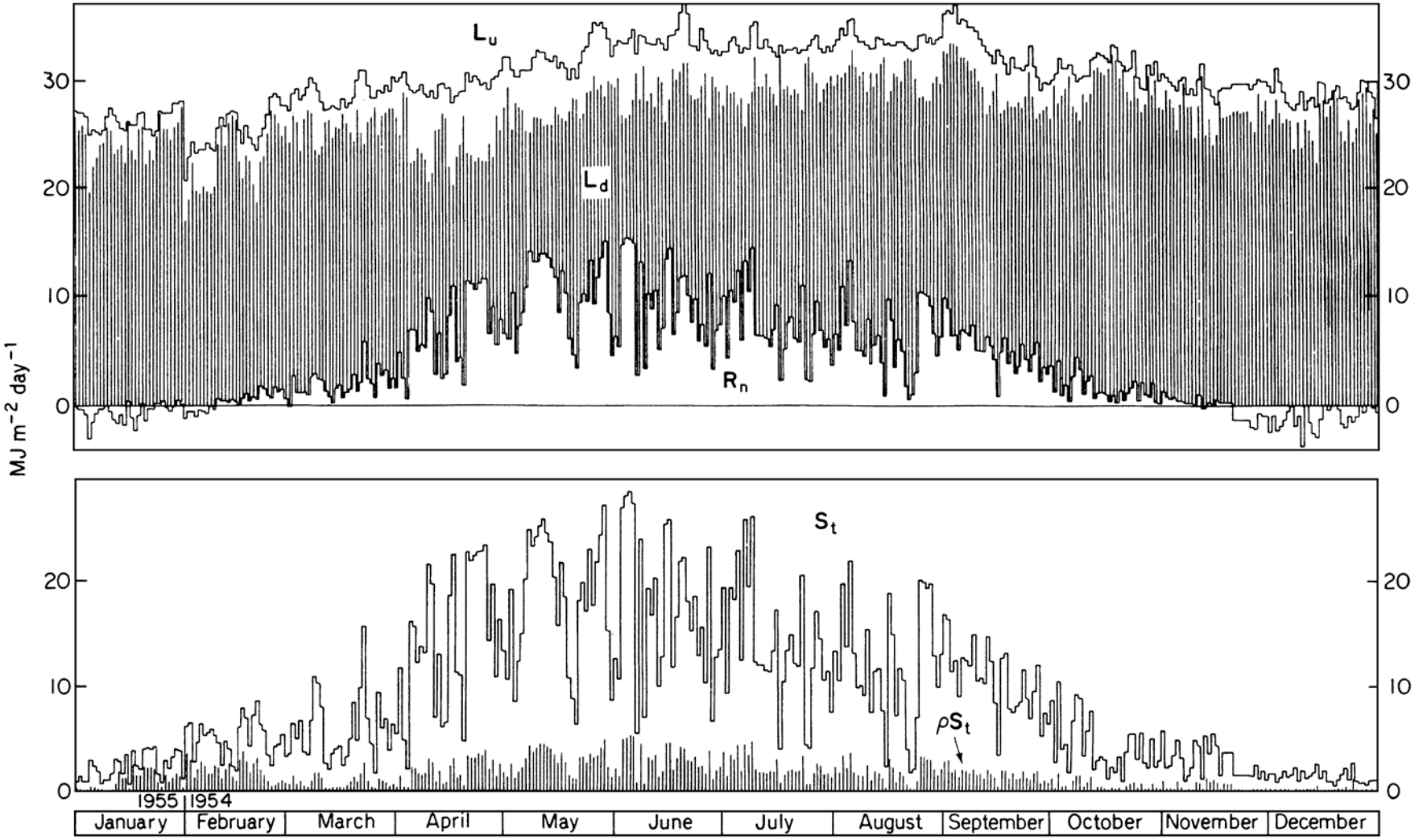

Figure 5.15 Annual radiation balance at Hamburg, Germany, 1954/55: $\mathbf{S}_t$, total solar radiation; $\rho\mathbf{S}_t$, reflected solar radiation; $\mathbf{L}_u$, upward long-wave radiation; $\mathbf{L}_d$, downward long-wave radiation; $\mathbf{R}_n$, net radiation (after Fleischer, 1955).

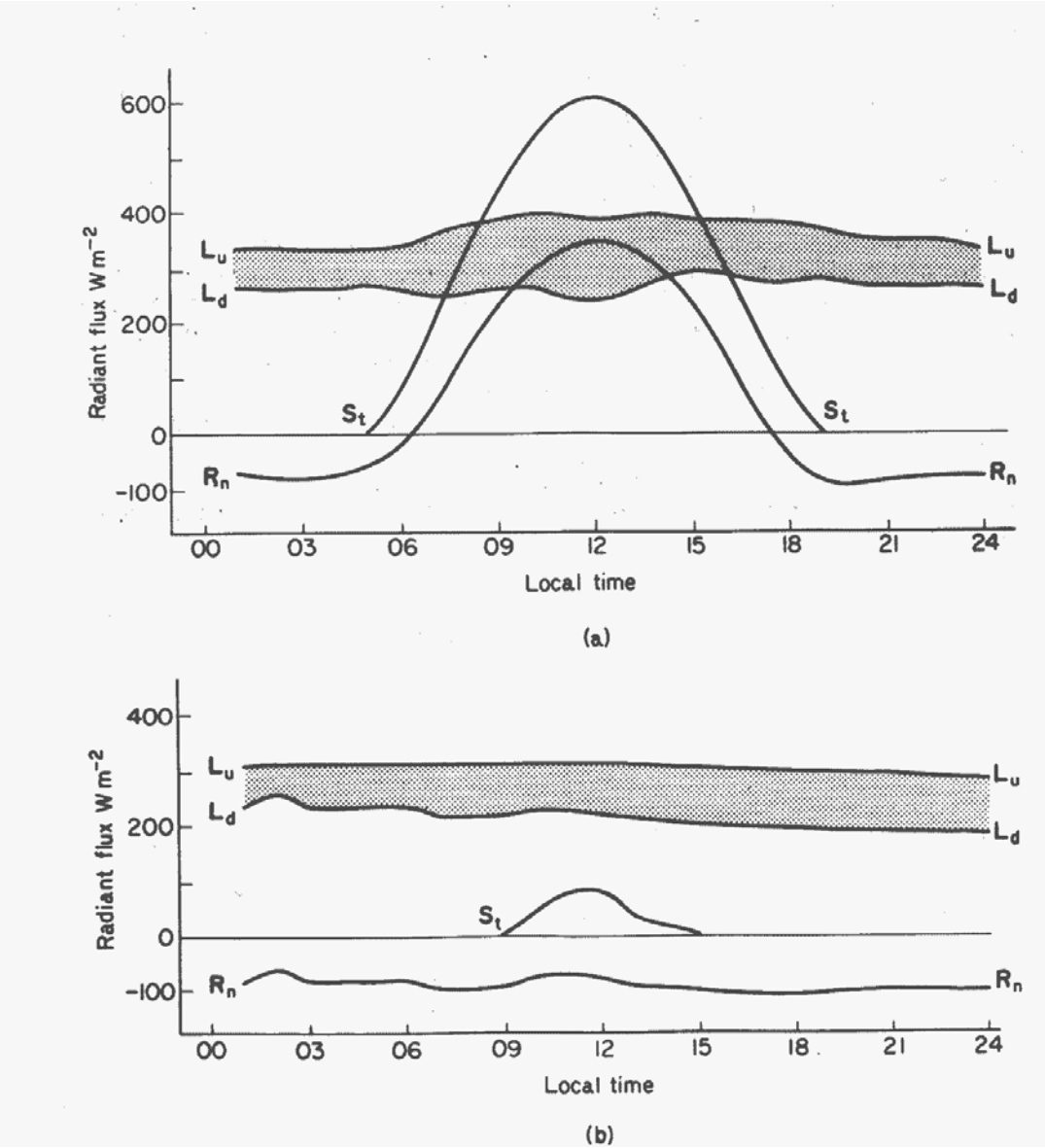

Figure 5.16 Radiation balance at Bergen, Norway (60°N, 5°E): (a) on 13 April 1968, (b) on 11 January 1968. The gray area shows the net long-wave loss and the line $\mathbf{R}_n$ is net radiation. Note that net radiation was calculated from measured fluxes of incoming short- and long-wave radiation, assuming that the reflectivity of the surface was 0.20 in April (e.g. vegetation) and 0.70 in January (e.g. snow). The radiative temperature of the surface was assumed equal to the measured air temperature.

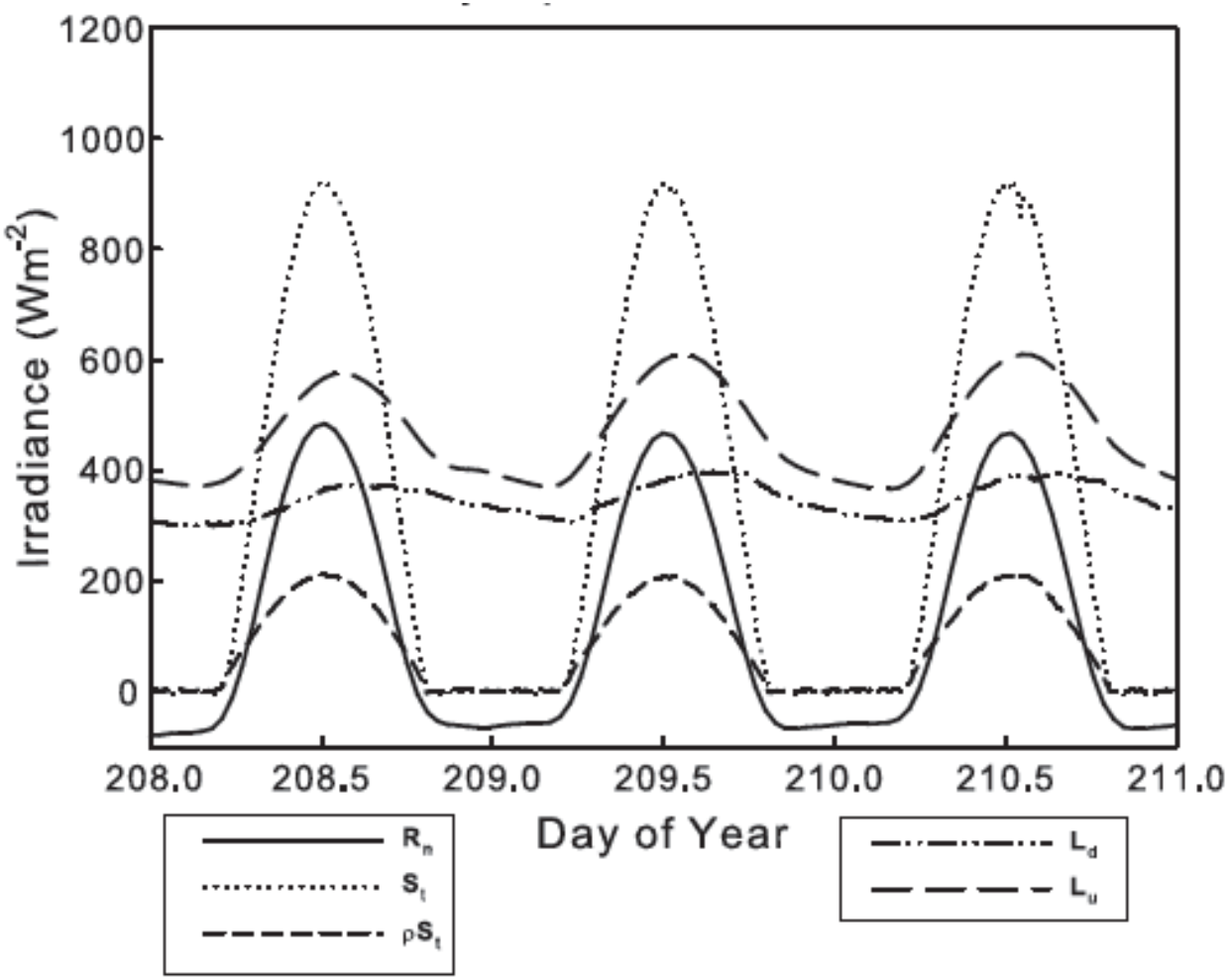

Figure 5.17 Components of the net radiation balance during three cloudless days over short grass near Corvallis, Oregon (45°N, 123°W). (data courtesy of Reina Nakamura, Oregon State University.)

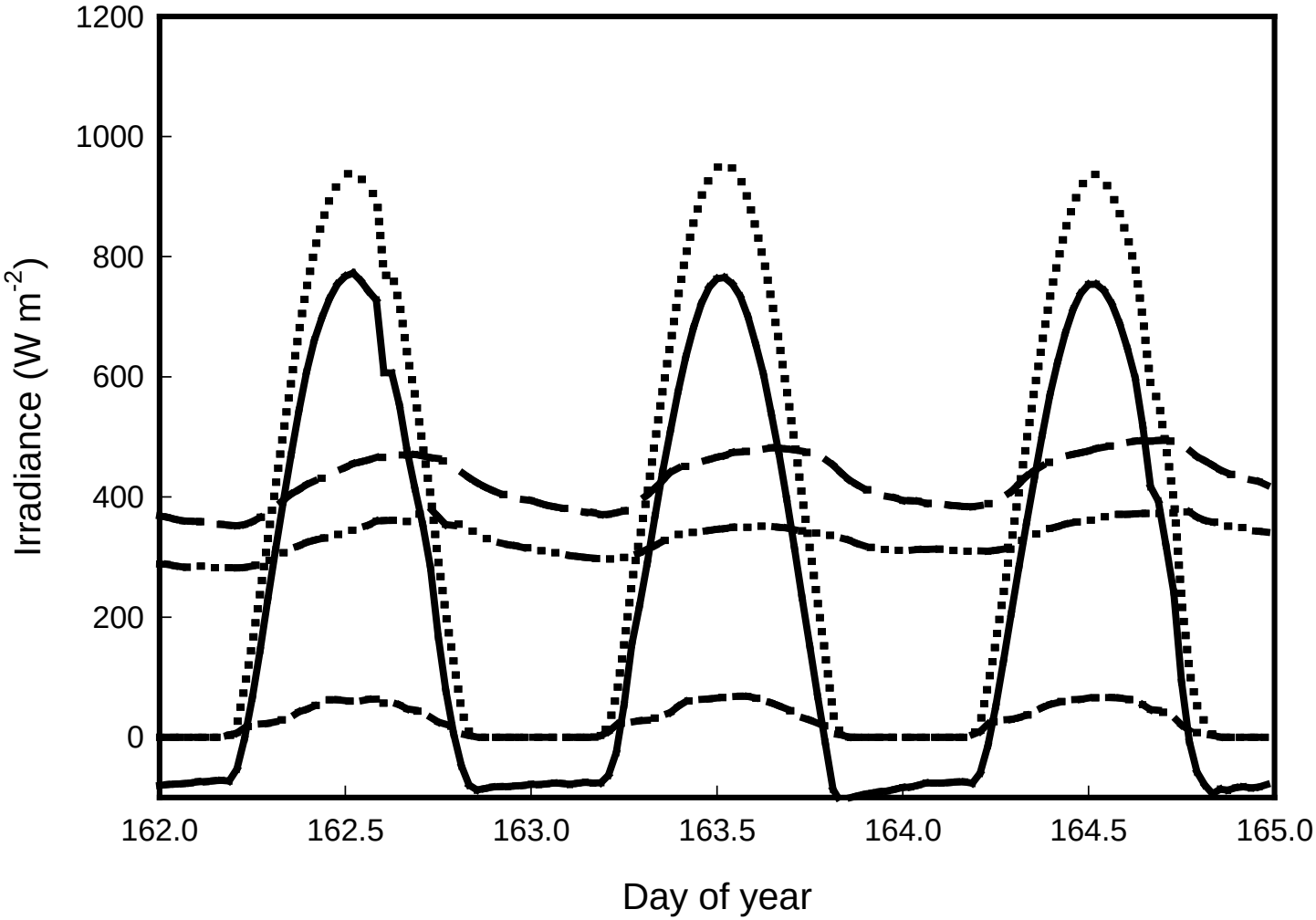

Figure 5.18 Components of the net radiation balance during three cloudless days over an old growth Douglas fir/Western Hemlock forest at Wind River Experimental Forest, Washington, (46°N, 120°W). Legends and line type are as in Fig. 5.17. (data courtesy of Ken Bible, University of Washington.)